Science Press

ARTICLE

Singularities of Contact Stress and Electric Field During Indentation of Piezoelectric Ceramics by Cylindrical, Flat Indenter

Chen Wenke[1,2],   Jin Wuyin[1]

[1] School of Mechanical and Electronic Engineering, Lanzhou University of Technology, Lanzhou 730050, China; [2] Mechanical Engineering, University of Kentucky, KY 40506, USA

Abstract: The finite element method (FEM) was used to simulate and to verify the axisymmetric nanoindentation response of a transversely isotropic piezoelectric ceramics by a conductive rigid flat indenter from half-space to thin film. The cylindrical, flat indenter without prescribed electric force was adopted to mechanically load the piezoelectric ceramics. The results show that the linear relationship between indentation load and indentation displacement is obtained. And the same relationship is obtained between electric potential and indentation displacement. In addition, resultant mechanoelectrical responses were analyzed. The simulation results indicate that the contact stress and electric field exhibit singularities round the edge of the indenter. Both stress and electric field singularities vary exponentially with respect to the thickness of the solids under the indenter. At the same time, the normal stress and electric potential distributions of the direct piezoelectric effects are given. Through the fitting formula of the normal stress, normal electric potential and tangential electric potential from the indentation interior to the contact edge under different indentation depths, the singular constants of electric field and stress field under different thickness of piezoelectric ceramics are proposed, and their variation rules are analyzed.

Key words: indentation; singularity; flat indenter; piezoelectric ceramics; stress; electric potential

Piezoelectric ceramics as efficient and clean energy materials have always attracted much concern. The research both on the macroscopic aspect (piezoelectric energy-harvesting tuned mass dampers[1] and high efficiency energy collector with small damping[2]) and micro aspects (novel piezoelectric nanogenerators[3] and multi-scale study of piezoelectric composites[4]) is very extensive. So, the design and characterization of advanced materials including piezoelectric ceramics are essential steps. Since the late 18th century, the indentation method is widely used for characterizing the mechanical properties of materials. The models of contact mechanics between indenters (flat, spherical, and conical) and half-space have been established[5,6]. In recent years, various indentation methods have been proposed. Zhao[7] modified the mechanical model of flat indentation system and established the equivalent film

thickness method. Yan[8] and Li[9] used nanoindentation experiments to study the behavior of materials. Wang[10] and Song[11] studied the length scale parameters of the contact stress and frictionless contact indentation. Wang[12] derived the frequency response function of thin film based on coupling stress. Campbell[13] has derived an analytical approximate solution for the indentation size effect of indenter. Liu[14] proposed an energy density equivalent method for indentation. The boundary element method was used to study the adhesive contact[15]. Similarly, many researches focused on indentation response of other materials, such as porous viscoelasticity, coating, rock, intermetallic compound[16-19]. Although the indentation responses of isotropic elastic materials have been well developed, the methods cannot be directly used in the nanoindentation of piezoelectric ceramic due to its unique properties.

Cylindrical indentation plays an important role in the design and characterization of advanced materials such as piezoelectric ceramics. Various theoretical methods have been proposed to study the indentation response of piezoelectric ceramics and structures. Giannakopoulos[20] presented a general theory on the indentation of piezoelectric half-space, and established explicit expressions for electromechanical responses of piezoelectric ceramics using the Hankel transform under a flat indenter. Nowacki[21] and Ding[22] employed the Green's functions to derive solutions for cylindrical, flat indentations of piezoelectric half-space. With the use of integral transform, Yang[23] has put forward the closed-form solution of axisymmetric indentation for a transversely isotropic piezoelectric ceramics by a conductive, cylindrical indenter. The indentation response of piezoelectric thin film under flat indenter has also been studied. For example, Wang[24,25] studied the axisymmetric indentation problem of a piezoelectric film perfectly bonded to a rigid substrate via the same method with Giannakopoulos. Makagon[26] further extended the investigation to the frictional sliding indentation of a piezoelectric film by a flat circular punch. Rodriguez-Tembleque[27] suggested that piezoelectric film is mainly reflected in different frictional contact boundary conditions. Wu[28] and Hou[29] conducted comprehensive studies on the mechanics of indentation for piezoelectric films on elastic substrate, under a charged flat indenter. The main contribution of Jin[30] is the theoretical study of axisymmetric contact and adhesive behavior of piezoelectric ceramics under a rigid flat indenter.

Indentation by a cylindrical, flat-ended indenter represents a classical contact mechanics problem due to the presence of stress singularity round the edge of the flat indenter[6,7,31]. The issue originated from the classic Boussinesq contact[32], which states that when one or both of the bodies has a discontinuous profile at the edge of the contact region, the stress concentrations or even intensifications will be expected at these singular points. In the indentation of an elastic solid by a cylindrical, flat indenter, it is demonstrated that the stresses in the solid will be singular near the edge of the indenter with an order of stress singularity equal to $-1/2$[31]. That is, the normal stress varies with the inverse square root of the radial distance. Several authors further postulated a quantitative equivalence between indentation contact mechanics and fracture mechanics since stress singularity factor K at the indenter contact tip is the same as the stress-intensity factor K_I in fracture mechanics[12,33].

The stress singularity in the indentation process of pure elastic half space has been well understood, and some researches focused on the singularity of interface free and singularity of contact between piezoelectric materials[34,35], but there are few researches on the singularity of the indentation of piezoelectric ceramics under flat indenter. The singularity of electric field leads to the stress singularity of indentation contact, which is easy to cause structural damage. As a result, the singularity analysis of the indentation of piezoelectric contact is vitally important. This work investigated both contact stress and electric field singularities during the indentation of piezoelectric ceramics by a cylindrical, flat indenter. And a wide range thickness of piezoelectric specimens was considered. Without any prescribed electric voltage, the indenter was mechanically loaded into the materials and the resultant mechanoelectrical responses were analyzed. The trends of indentation load, electric potential, and total charge on indentation depth were obtained for piezoelectric ceramics with varying thickness. The singularities of contact stress and electric field as a function of film thickness were also examined.

1 Problem Formulations

A transversely isotropic piezoelectric layer (thickness, t) loaded by a cylindrical, flat-ended indenter (radius, a) is shown in Fig. 1. It is further assumed that the piezoelectric layer is perfectly bonded to a rigid substrate. The cylindrical polar coordinate system (r, θ, z) is introduced because of the advantages that cylindrical materials are easier to define, the piezoelectric ceramics are isotopic and homogeneous in the r-θ plane and the direction of polarization is parallel to the z-axis. The contact between piezoelectric ceramics and indenter is treated as frictionless.

1.1 Governing equations

The origin of the coordinate system coincides with the surface center of the piezoelectric ceramics, and the z-axis points forward the piezoelectric ceramics. In the absence of any body sources and inertia forces, the equilibrium equations for the axisymmetric problem in Fig. 1 can be expressed as follows:

$$\frac{\partial \sigma_{rr}}{\partial r} + \frac{\partial \sigma_{rz}}{\partial z} + \frac{\sigma_{rr} - \sigma_{\theta\theta}}{\partial r} = 0 \tag{1}$$

$$\frac{\partial \sigma_{rz}}{\partial r} + \frac{\partial \sigma_{zz}}{\partial z} + \frac{\sigma_{rz}}{r} = 0 \tag{2}$$

Similarly, there is no body charge in the nanoindentation of piezoelectric ceramics, the electrostatic equation can be described as

$$\frac{\partial D_r}{\partial r} + \frac{D_r}{r} + \frac{\partial D_z}{\partial_z} = 0 \tag{3}$$

where, σ_{rr}, σ_{zz}, $\sigma_{\theta\theta}$, and σ_{rz} are the components of the stress tensor, D_r and D_z are the components of the electric displacement vector.

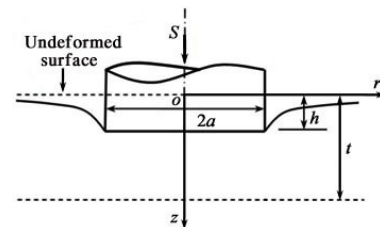To sum up, the constitutive equation of transversely isotropic piezoelectric ceramics with polarization direction

Fig.1   Schematic of the indentation of piezoelectric ceramics by a cylindrical flat indenter

parallel to the *z*-axis can be obtained as follows:

$$
\begin{Bmatrix} \sigma_{rr} \\ \sigma_{\theta\theta} \\ \sigma_{zz} \\ \sigma_{rz} \\ D_r \\ D_z \end{Bmatrix} = \begin{bmatrix} c_{11} & c_{12} & c_{13} & 0 & 0 & -e_{31} \\ c_{12} & c_{11} & c_{13} & 0 & 0 & -e_{31} \\ c_{13} & c_{13} & c_{33} & 0 & 0 & -e_{33} \\ 0 & 0 & 0 & c_{44} & -e_{15} & 0 \\ 0 & 0 & 0 & e_{15} & \in_{11} & 0 \\ e_{31} & e_{31} & e_{33} & 0 & 0 & \in_{33} \end{bmatrix} \begin{Bmatrix} \varepsilon_{rr} \\ \varepsilon_{\theta\theta} \\ \varepsilon_{zz} \\ 2\varepsilon_{rz} \\ E_r \\ E_z \end{Bmatrix} \quad (4)
$$

where, c_{11}, c_{12}, c_{13}, c_{33} and c_{44} are the piezoelectric elastic constants; e_{31}, e_{33} and e_{15} are the piezoelectric constants; $\in_{11}$ and $\in_{33}$ are the piezoelectric dielectric constants; ε_{rr}, $\varepsilon_{\theta\theta}$, ε_{zz}, and ε_{rz} are the components of the strain tensor; E_r and E_z are the components of the piezoelectric electric field intensity.

The relation between the strain and the displacement component u_r and u_z, and the relation between the electric field strength components and the electric potential (ϕ) can be expressed by the following equations:

$$
\varepsilon_{rr} = \frac{\partial u_r}{\partial r}, \varepsilon_{\theta\theta} = \frac{u_r}{r}, \varepsilon_{zz} = \frac{\partial u_z}{\partial z}, \varepsilon_{rr} = \frac{\partial u_z}{2\partial r} + \frac{\partial u_r}{2\partial z} \quad (5)
$$

$$
E_r = -\frac{\partial \phi}{\partial r}, E_z = -\frac{\partial \phi}{\partial z} \quad (6)
$$

Substituting Eq.(4~6) into Eq.(1~3) to obtain the governing equations with displacement components and electric potential as parameters:

$$
c_{11}\left(\frac{\partial^2 u_r}{\partial r^2} + \frac{1}{r}\frac{\partial u_r}{\partial r} + \frac{u_r}{r^2}\right) + c_{44}\frac{\partial^2 u_r}{\partial r^2} + (c_{13}+c_{44})\frac{\partial^2 u_z}{\partial r\partial z}
$$
$$
+ (e_{15}+e_{31})\frac{\partial^2 \phi}{\partial r\partial z} = 0 \quad (7)
$$

$$
c_{44}\left(\frac{\partial^2 u_z}{\partial r^2} + \frac{1}{r}\frac{\partial u_z}{\partial r}\right) + c_{33}\frac{\partial^2 u_z}{\partial z^2} + (c_{13}+c_{44})
$$
$$
\left(\frac{\partial^2 u_z}{\partial z\partial r} + \frac{1}{r}\frac{\partial u_r}{\partial z}\right) + e_{15}\left(\frac{\partial^2 \phi}{\partial r^2} + \frac{1}{r}\frac{\partial \phi}{\partial r}\right) + e_{33}\frac{\partial^2 \phi}{\partial z^2} = 0 \quad (8)
$$

$$
e_{15}\left(\frac{\partial^2 u_z}{\partial r^2} + \frac{1}{r}\frac{\partial u_z}{\partial r}\right) + e_{33}\frac{\partial^2 u_z}{\partial z^2} + (e_{15}+e_{31})\left(\frac{\partial^2 u_r}{\partial z\partial r} + \frac{u_z}{r}\right)
$$
$$
- \in_{11}\left(\frac{\partial^2 \phi}{\partial r^2} + \frac{1}{r}\frac{\partial \phi}{\partial r}\right) - \in_{33}\frac{\partial^2 \phi}{\partial z^2} = 0 \quad (9)
$$

According to the actual contact condition of piezoelectric ceramics indentation, the relationship between the penetration depth *h* and the contact radius *a* is given through continuity contact condition. Assuming that the contact pressure of indentation is $p(r)$, $p(r) = -\sigma_{rr}(r,0)$ and the indentation force *P* can be calculated as

$$
P = 2\pi \int_0^a r p(r) \, dr \quad (10)
$$

The electric charge distribution under the indenter is $q(r) = -D_z(r,0)(0 \leq r \leq a)$, and the total electric charge *Q* under the conducting indenter can be found by integrating $q(r)$:

$$
Q = 2\pi \int_0^a r q(r) \, dr \quad (11)
$$

1.2 Boundary conditions

1.2.1 Mechanical boundary conditions

A rigid, frictionless indenter is normally indented to the transversely isotropic piezoelectric ceramics by applying displacement loading along *z*-axis, namely *S* in Fig. 1. It is assumed that the indenter is monotonically pressed into the piezoelectric ceramics with *S*. *h* is the indentation depth from the initially surface.

In the contact region of *r*<*a*, due to the rigid and frictionless flat indenter profile, the mechanical boundary conditions must satisfy the normal displacement. The *z*-axis displacement of flat indenter can be approximated by

$$
u_z(r,0) = h \quad (12)
$$

The *z* direction displacement in the contact area is $u_z(a,0)$, and the contact boundary between the indenter and the piezoelectric ceramics has two situations, namely the pile-up, $u_z(a,0) > 0$, or sink-in, $u_z(a,0) < 0$.

There is no frictional traction, and normal tractions equal zero outside the contact region.

$$
\sigma_{rz}(r,0) = 0, r \geq 0 \quad (13)
$$

$$
\sigma_{zz}(r,0) = 0, r > 0 \quad (14)
$$

Assuming that the deformation at the contact boundary between the contact area and the out of is smooth, the continuity condition of the contact boundary is

$$
du_z(r=a-, z=0)/dr = du_z(r=a+, z=0)/dr, r=a \quad (15)
$$

1.2.2 Electrical boundary conditions

The electrical boundary conditions are determined by the conductivity of the indenter. For the case of the perfect conducting indenter with potential ϕ_0, the potential of the indenter will be the same as that of the deformed contact surface of the piezoelectric ceramics indentation. The electric potential needs to be determined by solving the contact deformation because the potential depends on the indentation depth and the surface profile of the indenter.

$$
\phi(r,0) = \phi_0, r \geq 0 \quad (16)
$$

$$
D_z(r,0) = 0, r > a \quad (17)
$$

2 Finite Element Simulation

Indentation deformation of a transversely isotropic piezoelectric ceramics by a flat, cylindrical indenter is simulated and analyzed by ANSYS. An axisymmetric analysis model is used and PLANE223 is selected, referring to the selection criteria of simulation parameters in Ref.[27,36]. The conductive, flat indenter with a radius of *a*=1 μm is modeled as rigid. If the length of material is 10 times larger than the radius of indenter, indentation effect can be negligible. The piezoelectric ceramics have a width of 15 μm and variation thicknesses *t* of 15, 10, 5, 2, 1, 0.5, 0.2, 0.1, 0.05, 0.03, 0.025, 0.020, and 0.015 μm. So the normalized thickness (*a/t*) of the piezoelectric ceramics varies in the range of 0.067 to 66.7.

Fig. 2 shows the finite element mesh of a 15 μm×15 μm piezoelectric specimen. The mesh consists of 117 168 eight-node axisymmetric elements using local mesh refinement method. Contact elements are used at the interface of indenter and piezoelectric layer, and the change of the contact area in the indentation process can be intuitively understood. The displacement is used as the load in ANSYS simulation. The indenter is gradually close to the surface of the piezoelectric
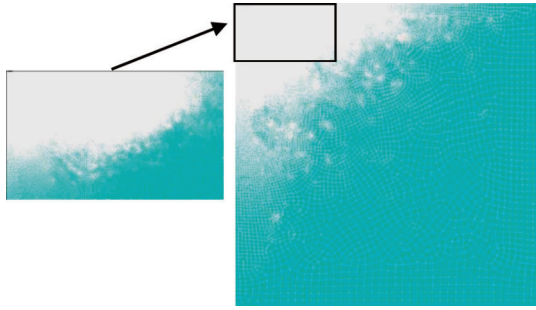
Fig.2　Finite element mesh of a typical indenter-piezoelectric solid system

Fig.3　Distributions of displacement (a) and electric potential (b) in PZT-4 under a cylindrical flat indenter

ceramics, then contacts with the surface and is pressed through displacement-controlling to reach the preset indentation depth; finally put back the indenter to its original position. For the conducting indenter, the nodes in the contact region are equipotential, and the nodes of the contact interface between the piezoelectric ceramics and the substrate are constrained by zero electric potential. The piezoelectric structure used in the analysis is PZT-4, a transversely isotropic material with the properties shown in Table 1.

3　Results and Discussion

3.1　Indentation of piezoelectrical half-space

The PZT-4 in a wide range thickness are modeled in this work. The normalized thickness (a/t) of the PZT-4 varies from 0.067 to 66.7. As the contact radius (i. e., the indenter radius for a flat indenter) is sufficiently small compared to the solid thickness, typically $a/t < 1/10^{th}$, the effect of substrate beneath on the piezoelectric layer can be neglected and the indentation of piezoelectric layer in a finite thickness may be equivalent to the indentation of a solid with infinite thickness. Unlike most studies reported that the indenters are electrically charged[20,23,24], the present work exerts only displacement loading (S) at the indenter and then observes the mechanoelectrical responses in the PZT-4. Fig. 3a and 3b show the distributions
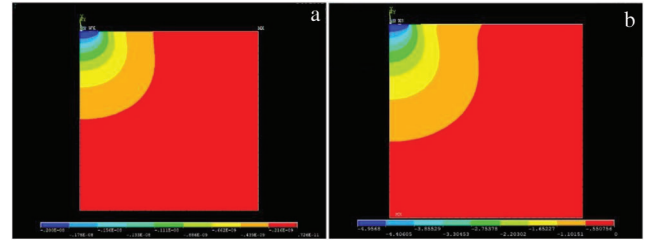
of displacement and electric potential in PZT-4 (a/t=0.067). It is roughly the same as the contour image of flat indentation simulated by COMSOL Multiphysics in Ref. [37]. The area where the displacement and potential change sharply mainly occurs under the indenter and then propagates outwards to a distance of ~$5a$. Both displacement and potential diminish at the far field, indicating that the influence of substrate beneath the piezoelectric material is negligible when the thickness of the piezoelectric material exceeds a limit.

The relationships between indentation load-depth and electric charge-depth for the axisymmetric indentation of transversely isotropic PZT-4 have been extensively studied and the solutions are given as [20,24]

$$P = 4C_1 a\left(h + C_2\phi_1\right) \tag{18}$$

$$Q = 4C_3 a\left(h + C_4\phi_1\right) \tag{19}$$

where C_1, C_2 C_3, C_4 are coefficients that can be computed from fundamental elastic and piezoelectric constants shown in Table 1. Detailed formulas for computing C_i are available in Ref.[24]. Using the data in Table 1, the theoretical P-h and Q-h responses are computed for the present PZT-4 and plotted against with computational simulations (Fig.4a and 4b). It can be seen that there is excellent agreement between the FEM and the theoretical solutions, indicating that the procedures used in the finite element modeling of present indenter piezoelectric system are accurate.

Table 1　Material properties of PZT-4[36]

Elastic constant/×10^{10}N·m^{-2}					Piezoelectric constant/C·m^{-2}			Dielectric constant/×10^{-9}F·m^{-1}	
c_{11}	c_{12}	c_{13}	c_{33}	c_{44}	e_{31}	e_{33}	e_{15}	$\in_{11}$	$\in_{33}$
13.9	7.78	7.43	11.3	2.56	−6.98	13.84	13.44	6.00	5.47

Using the FEM, the indentation load-depth and electrical charge-depth responses of a piezoelectric half-space under a conducting, flat indenter are obtained and depicted in Fig. 4a and 4b, respectively. In these plots, the indentation depth is normalized with indenter radius; the load and electrical charge is normalized with the value at initial contact. The maximum error between the FEM simulation results and results obtained by Eq. (18) and Eq. (19) appears at the maximum indentation. The indentation force is basically the same, and the total charge error is about 0.4%. The resultant load and electrical charge responses are linear, consistent with findings reported
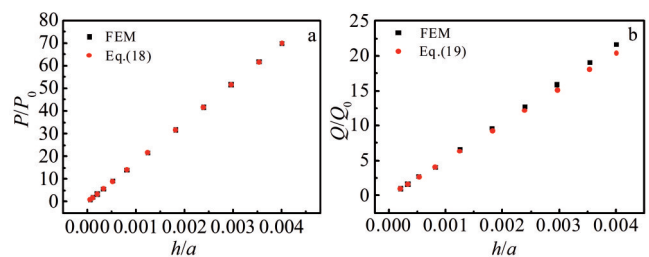

Fig.4　Indentation load-depth curve (a) and indentation electrical charge-depth curve (b) of a piezoelectrical half-space

in the Ref.[24,36].

3.2 Singularities in piezoelectric half-space

There are singularities of mechanical stress and electric field at the position where the radial displacement of PZT-4 is equal to a. The contours of contact stress and electric field in a piezoelectric half space are obtained by FEM, as shown in Fig. 5a and 5b, respectively. During the indentation process, both contact stress and electric field are concentrated round the edge, which indicates that there are obvious singular points under the unique indenter. This is the same singularity as Ref.[38], because the surface of the piezoelectric material is not smooth.

The distributions of contact stress σ_{zz} and electric field E_z in the PZT-4 are plotted along the radial direction (r), as shown in Fig. 6a and 6b. The spots of the same color represent the stress and electric field distribution values on the contact surface of the piezoelectric material under the same indentation depth. This is the same in the following figures and will not be repeated. The stress and electric displacement of the internal contact are approximately equivalent, and the

closer to the edge, the greater the strength of the stress and electric field. t=15 000 nm represents half-space, as stress and electric field are coupled to each other, and the singularity of stress field leads to the sudden change of electric field. The variation trend of contact stress and electric field in Fig. 6 is highly consistent with the results in Ref. [24, 25, 38]. Both quantities seem to be uniform at the center of the indenter and then to increase to infinities round the edge (r-a> =10^{-6} m). According to the fitting formula, both normal stress σ_{zz} and electric filed E_z vary inversely with respect to the square root of the radial distance (r), i.e., $\sigma_{zz} \sim K_S \cdot (a^2 - r^2)^{-1/2}$, $E_z \sim K_E \cdot (a^2 - r^2)^{-1/2}$, where K_S and K_E are considered to be the stress and electric filed singularity constants occurred in indentation. By plotting σ_{zz} vs $(a^2 - r^2)^{-1/2}$ and E_z vs $(a^2 - r^2)^{-1/2}$, K_S and K_E can be obtained (the slopes of the two plots). It is seen from Fig. 7a and 7b that the singularity constants increase linearly with the depth of indentation (h). In this work, the singular parameters include all parameters except the square root of the second order, and both the indentation force and charge change linearly with the indentation depth (Fig. 4), which corresponds to the slope change trend of the singular parameters, and the result shows that it is correct.

3.3 Influence of PZT-4 thickness on the field singularity

In present study, the indentation responses of 13 kinds of PZT-4 with different thicknesses are modeled. Then, the variation of contact stress and electric field singularity in indentation response is focused on. The normalized thickness (indenter radius/sample thickness, a/t) is varied over a range of 0.067 to 66.7. As the indenter radius (contact radius) is sufficiently larger than the sample thickness, i.e., a/t >10th, the influence of the substrate underneath the sample can be ignored and the indentation responses of a testing sample are similar to those of a half space. However, as the normalized thickness is large, the indentation responses of the testing samples are complex and analytical solutions merely exist.

Fig. 8 shows the contours of stress σ_{zz} and electric fields E_z of PZT-4 with the normalized thickness a/t=1 and a/t=67. Only part of the PZT-4 near the indentation is shown in Fig.8a and 8b. The stress and electric field at the edge of the indenter change obviously, which are exactly the same as the stress-strain figure of the flat indenter in Ref.[39]. At about t=1000 nm, the stress change of the indentation surface only appears in the range of radius less than a. At the edge position, the
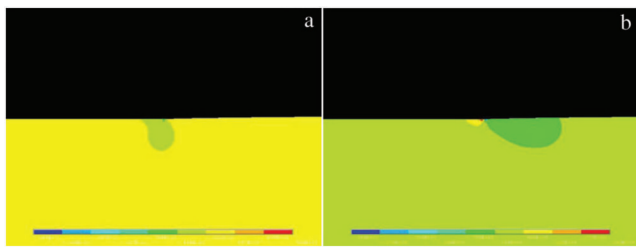

Fig.5　Field distributions in a piezoelectrical half-space: (a) normal stress and (b) z direction electric field
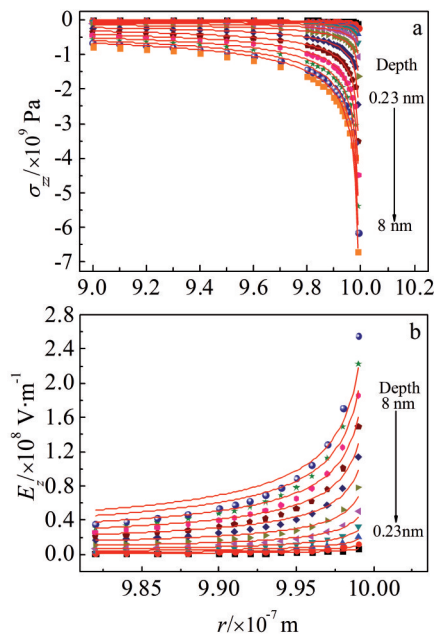

Fig.6　Effects of indentation depth on distributions of mechanical and electrical fields in a piezoelectrical half-space: (a) normal stress and (b) z direction electric field

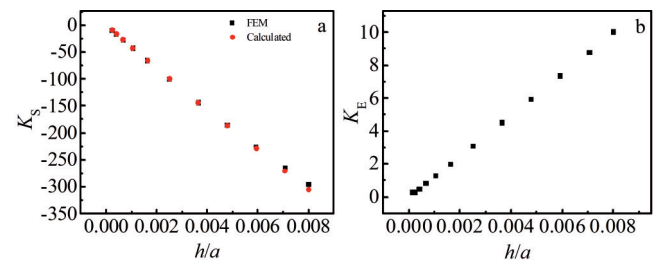Fig.7　Effect of indentation depth on constants K_S and K_E: (a) normal stress and (b) z direction electric field
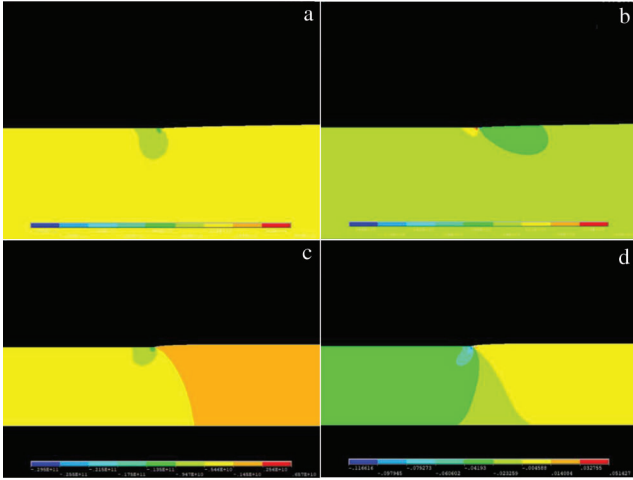
Fig.8   Distributions of contact stress σ_{zz} (a, c) and electric field E_z (b, d) in piezoelectric solids: (a, b) a/t=1 (t=1000 nm) and (c, d) a/t= 67 (t =15 nm)

stress value increases abnormally, which indicates that the color in the figure is deepened. In the PZT-4, there is a circular gradient decreasing trend along the direction of indentation depth. Due to the deformation of elastic PZT-4, there are also moving electrons in the range larger than *a*, so, a relatively weak symmetrical field appears outside the indentation. In the piezoelectric film represented by *t*=15 nm, the change of stress inside the indentation is consistent with the half infinite space, but the normal stress which is outside the indentation is smaller than that inside the indentation, and this is consistent with the fault in the figure. The results show that the variation of the electric field is affected by the thickness of the PZT-4. The electric field intensity of the

singular point is significantly higher than other places, and the distribution of electric field intensity inside and outside the indentation is different. The reason for the singularity of stress and electric field is the discontinuity of PZT-4 surface due to flat indentation.

The distribution fitting of contact stress and electric field is plotted along the indenter face (*r* direction), as shown in Fig.9. Again, both σ_{zz} and E_z appear to be uniform in the center of the punch and then to increase rapidly with respect to *r*. Both of these quantities are seen to approach to infinities round the edge of the indenter. In approximately half-space, the quadratic root is used to fit the normal stress and normal electric field at different indentation depth, and the fitting curve is highly coincident with the field strength. In the case of piezoelectric film, using the same fitting method, the coincidence degree decreases at the position far away from the singularity. These two cases coincide with Fig. 8, indicating the change law of the composite square root of the field strength of the PZT-4 in the semi-infinite space. The piezoelectric film is affected by the substrate due to its small thickness, and the square root of the second order fitting condition can only be satisfied at the position very close to the singular point.

Although the variation trend of the total contact stress and electric field in Fig.9 is consistent with the results of Ref.[24, 38,40], in the case of infinite film, the normal stress and the normal electric field intensity on the whole surface of the contact area are closer to the sum of the variable constant and the singular factor multiplied by the square root. The variable constants are related to indentation depth and thickness.

By plotting σ_{zz} vs $(a^2 - r^2)^{-1/2}$ and E_z vs $(a^2 - r^2)^{-1/2}$, singularity constants K_S and K_E are estimated (Fig.10). Similar to the trends observed in the piezoelectric half space (Fig.7),
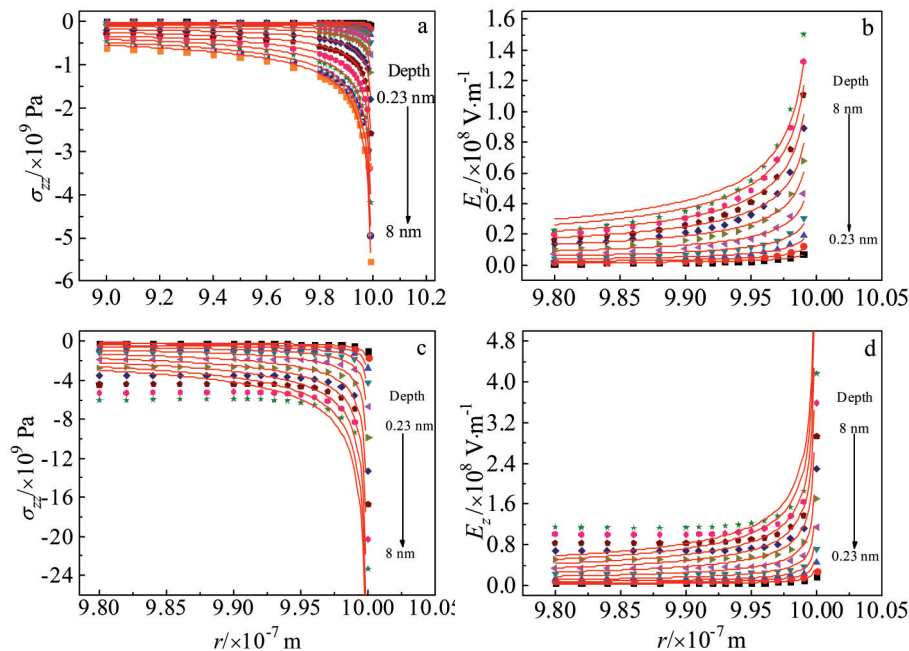

Fig.9   Effects of PZT thickness on distributions of contact stress σ_{zz} (a, c) and electric field E_z (b, d) in PZT-4: (a, b) a/t=1 (t=1000 nm) and (c, d) a/t=67 (t=15 nm)
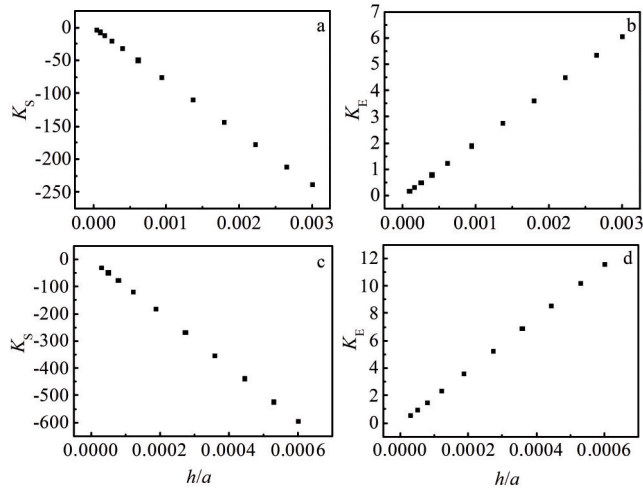
Fig.10   Effects of PZT thickness on singularity constants K_S and K_E of contact stress σ_{zz} (a, c) and electric field E_z (b, d) in PZT-4: (a, b) a/t=1 (t=1000 nm) and (c, d) a/t =67 (t=15 nm)

both K_S and K_E vary linearly with respect to the depth of indentation (h/a) for PZT-4 at finite thickness (a/t=1 and a/t= 67). The deeper the indentation, the larger the singular constant, which is consistent with the transverse isotropy of the material[25,37]. However, the magnitudes of singularity constants K_S and K_E seem to vary with the sample thickness: the smaller the sample thickness, the higher the singularity values. By comparing the thickness of 13 kinds of PZT-4, the thinner the material, the higher the singular factor of stress and electric field.

3.4 Indentation parameters for different thickness

To comprehensively examine the effect of sample thickness, finite element simulations are performed on PZT-4 over a wide range of thickness and the resultant mechanoelectrical responses are analyzed. First, the indentation load-depth and electric charge-depth responses are analyzed for PZT-4 with different thicknesses. The slope of each load-depth or electric charge-depth curve is calculated in Ref.[24] and simulated for each sample and then plotted as a function of sample thickness (a/t), as shown in Fig.11a. The slope of each electric charge-depth curve is simulated by FEM and then plotted in Fig.11b. The slope can be considered as a measure of the "stiffness" of mechanical load-depth or electric charge-depth response. Overall such "stiffness" varies in exponential fashions. The indentation force is sensitive to
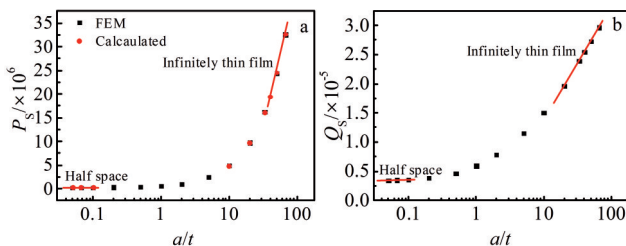

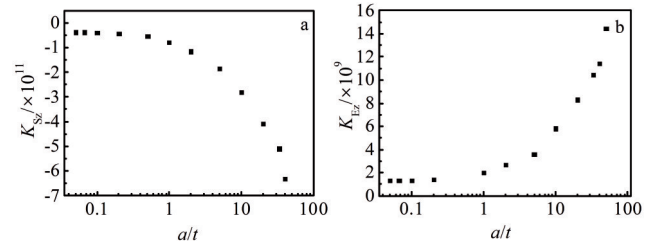Fig.11   Slope of force-depth (a) and total charge-depth (b) as a function of a/t

Fig.12   Thickness-dependency of slope of singularity constants K_{Sz} (a) and K_{Ez} (b)

the thickness of the PZT-4, especially in the film state. The variation trend of charge depending on the thickness of the PZT-4 is the same as that of the indentation force, but it is very slow. The two red lines represent a half-space and an infinitely thin film. In addition to FEM results (black spots), the theoretical predictions are added at the two asymptotes which correspond to piezoelectric half space and infinitely thin piezoelectric film. For these two extreme cases, closed-form solutions have been established[25,30]. It is seen that the numerical results agree well with the closed-form solutions for PZT-4 in very small and very large thickness.

In the fitting of electric field intensity E_z and E_r vs ($a^2 - r^2$)$^{-1/2}$, the singular factors of electric field intensity varying with the indentation depth in the indentation process of PZT-4 with different thickness are extracted firstly. After calculating the slope of the singular factors, the variation trend of normal and tangential electric field singular factors with the thickness can be obtained. It can be summed up intuitively, and the variation of electric field intensity singular factors can be ignored only in the half infinite space (Fig. 12). Both stress and electric field singularities exhibit a strong dependency on the thickness of the piezoelectric samples. It is obvious that the electric field singularity factor changes dramatically in the case of thin film, which is not only related to the indenter shape and indentation depth, but also concerned to the substrate, because the interface in the piezoelectric film structure has a great influence on the performance[29]. Similar to the trends observed in the stiffness (Fig.10), the singularity constants (K_S and K_E) increase inversely with sample thickness in an exponential manor. The transitions seem to occur at around a/t=0.2. As the thickness is less than ~0.2, the material under the indenter behaves like a solid of infinite thickness and the singularity values remain relatively unchanged. When the thickness is greater than ~0.2, the materials start to transit to thin films and the effect of the substrate becomes significant, causing significant increase in stress or electric charge singularities round the indenter edge.

4 Conclusions

1) Both contact stress and electric field exhibit singularities round the edge of the indenter. By curve fitting of the stress and electric field along the radial direction (r), the relevant singularity constants, K_S and K_E, can be obtained, which vary linearly with the depth of indentation (h).

2) The singularity issues occurring originally in infinite elastic medium are highly correlated with the material thickness according to the finite element model results. Both stress and electric field singularities vary exponentially with respect to the thickness of the solids under the indenter. The singularity constants (K_S and K_E) derived from piezoelectric half space may remain unchanged as the sample thickness (a/t) is less than ~0.2.

References

1   Pan P, Zhang D B, Nie X *et al*. *Science China Technological Sciences*[J], 2017, 60(3): 467

2   Khazaee M, Huber J E, Rosendahl L *et al*. *Applied Energy*[J], 2021, 285: 116 427

3   Sam A, Natraj V, Marappan G *et al*. *Materials Letters*[J], 2021, 294: 129 798

4   Uetsuji Y, Wada T, Tsuchiya K. *Computational Materials Science*[J], 2019, 158: 159

5   Sneddon I N. *International Journal of Engineering Science*[J], 1965, 3(1): 47

6   Johnson K L. *Contact Mechanics*[M]. Cambridge: Cambridge University Press, 1985: 214

7   Zhao Xiang, Wang Fenghui, Guo Zhangxin *et al*. *Rare Metal Materials and Engineering*[J], 2012, 41(12): 2223 (in Chinese)

8   Yan Wuzhu, Li Youliang, Wen Zhixun *et al*. *Rare Metal Materials and Engineering*[J], 2020, 49(6): 1854 (in Chinese)

9   Li Chunyan, Zhu Fuping, Ding Juanqiang *et al*. *Rare Metal Materials and Engineering*[J], 2020, 49(10): 3353

10 Wang Y X, Shen H M, Zhang X *et al*. *International Journal of Solids and Structures*[J], 2018, 138: 76

11 Song H X, Ke L L, Wang Y H *et al*. *International Journal of Applied Mechanics*[J], 2018, 10: 1 850 049

12 Wang Y X, Zhang X, Shen H M *et al*. *International Journal of Solids and Structures*[J], 2020, 191-192: 449

13 Campbell C J, Gill S. *International Journal of Solids and Structures*[J], 2019, 171: 81

14 Liu X, Cai L, Chen H *et al*. *Chinese Journal of Aeronautics*[J], 2020, 33(12): 3266

15 Wu J J. *Journal of Adhesion Science and Technology*[J], 2020, 34(21): 2292

16 Lin Y Y. *International Journal of Solids and Structures*[J], 2019, 190: 291

17 Stepanov F I, Torskaya E V. *Journal of Friction and Wear*[J], 2019, 40(4): 326

18 Zhang L G. *Open Geosciences*[J], 2018, 10(1): 289

19 Staszczyk A, Sawicki J, Koodziejczyk U *et al*. *Coatings*[J], 2020, 10(9): 846

20 Giannakopoulos A E, Suresh S. *Acta Materialia*[J], 1999, 47(7): 2153

21 Nowacki J P. *Green's Functions for Piezoelectric Strip with a General Line Source*[M]. Berlin: Springer Berlin Heidelberg, 2006: 125

22 Ding H J, Chen Buo, Liang J. *International Journal of Solids and Structures*[J], 1996, 33(16): 2283

23 Yang F Q. *Journal of Applied Physics*[J], 2008, 103(7): 74 115

24 Wang J H, Chen C Q, Lu T J. *Journal of the Mechanics and Physics of Solids*[J], 2008, 56(12): 3331

25 Wang B L, Han J C. *Archive of Applied Mechanics*[J], 2006, 76(7-8): 367

26 Makagon A, Kachanov M, Karapetian E *et al*. *International Journal of Engineering Science*[J], 2009, 47(2): 221

27 Rodriguez-Tembleque L, Saez A, Aliabadi M H. *International Journal of Engineering Science*[J], 2016, 107: 36

28 Wu Y F, Yu H Y, Chen W Q. *International Journal of Solids and Structures*[J], 2012, 49(1): 95

29 Hou P F, Zhang W H. *Meccanica*[J], 2019, 54(15): 2461

30 Jin F, Yan S P, Guo X *et al*. *Mechanics of Materials*[J], 2018, 129: 189

31 Muskhelishvili N I. *Some Basic Problems of the Mathematical Theory of Elasticity*[M]. Holland: Springer Dordrecht, 1954: 450

32 Fu G H, Cao L. *Journal of Materials Science*[J], 2008, 62(2): 3063

33 Barquins M, Maugis D. *Journal de Mecanique Theorique et Appliquee*[J], 1982, 1(2): 331

34 Shang F, Kitamura T. *Microsystem Technologies*[J], 2005, 11: 1115

35 Jiang L, Ge R Y, Zhang J L. *Mathematical Problems in Engineering*[J], 2020, 5 616 138

36 Liu M, Yang F Q. *International Journal of Solids and Structures*[J], 2013, 50: 2542

37 Campbell C J, Gill S. *International Journal of Solids and Structures*[J], 2019, 171: 8

38 Li X, Zhou Y T, Zhong Z. *Applied Mathematics and Physics*[J], 2015, 66(2): 473

39 Dean J, Clyne T W. *Mechanics of Materials*[J], 2017, 105: 112

40 Volkov S S, Vasiliev A S, Aizikovich S M *et al*. *Acta Mechanica*[J], 2019, 230(4): 1289

圆柱平压头压电陶瓷压痕过程中接触应力和电场的奇异性

陈文科[1,2]，靳伍银[1]

(1. 兰州理工大学 机电工程学院，甘肃 兰州 730050)

(2. 肯塔基大学 机械工程系，美国 肯塔基州 40506)

摘　要：采用有限元方法，针对横观各向同性压电材料进行轴对称纳米压痕的机电耦合响应数值仿真。结果表明：当压入过程中不施加预设电压，压痕载荷与压痕位移之间呈线性关系；导电压头上电势与压痕位移也呈相似关系，压头边缘附近的接触应力和电场存在奇异性，且二者均随压头下固体厚度呈指数变化。通过对不同压痕深度和材料厚度下，从压头内部到接触边缘径向应力、法向电势和切向电势分布情况的拟合公式得到了不同压电材料厚度下电场和应力场的奇异常数，并对其变化规律进行了分析。

关键词：压痕；奇异性；平头压头；压电陶瓷；应力；电势

作者简介：陈文科，男，1990 年生，博士，兰州理工大学机电工程学院，甘肃 兰州 730050，E-mail：Chenwk0722@outlook.com